BRG1 promotes transcriptional patterns that are permissive to proliferation in cancer cells

Authors:

Katherine A. Giles[1,2,3], Cathryn M. Gould[1], Joanna Achinger-Kawecka[1,4], Scott G. Page[2], Georgia Kafer[2], Phuc-Loi Luu[1,4], Anthony J. Cesare[2], Susan J. Clark[1,4]*, Phillippa C. Taberlay[3]*

*These authors contributed equally

Affiliations:

[1]Epigenetics Research Laboratory, Genomics & Epigenetics Theme, Garvan Institute of Medical Research, Sydney, NSW, 2010, Australia

[2]Genome Integrity Unit, Children's Medical Research Institute, University of Sydney, Westmead, NSW, 2145, Australia

[3]Tasmanian School of Medicine, College of Health and Medicine, University of Tasmania, Hobart, TAS, 7000, Australia

[4]St Vincent's Clinical School, UNSW Sydney, Sydney, NSW, 2000, Australia

Correspondence: Phillippa C. Taberlay (phillippa.taberlay@utas.edu.au)

ABSTRACT

Background: BRG1 (encoded by *SMARCA4*) is a catalytic component of the SWI/SNF chromatin remodelling complex, with key roles in modulating DNA accessibility. Dysregulation of BRG1 is observed, but functionally uncharacterised, in a wide range of malignancies. We have probed the functions of BRG1 on a background of prostate cancer to investigate how BRG1 controls gene expression programs and cancer cell behaviour.

Results: Our investigation of *SMARCA4* revealed that BRG1 is universally overexpressed in 486 tumours from The Cancer Genome Atlas prostate cohort, as well as in a complementary panel of 21 prostate cell lines. Next, we utilised a temporal model of BRG1 depletion to investigate the molecular effects on global transcription programs. Unexpectedly, depleting BRG1 had no impact on alternative splicing and conferred only modest effect on global expression. However, of the transcriptional changes that occurred, most manifested as down-regulated expression. Deeper examination found the common thread linking down-regulated genes was involvement in proliferation, including several known to increase prostate cancer proliferation (*KLK2*, *PCAT1* and *VAV3*). Interestingly, the promoters of genes driving proliferation were bound by BRG1 as well as the oncogenic transcription factors, AR and FOXA1. We also noted that BRG1 depletion repressed genes involved in cell cycle progression and DNA replication but intriguingly, these pathways operated independently of AR and FOXA1. In agreement with transcriptional changes, depleting BRG1 conferred G1 arrest.

Conclusions: Our data have revealed that BRG1 has capacity to drive oncogenesis by coordinating oncogenic pathways dependent on BRG1 for proliferation, cell cycle progression and DNA replication.

Keywords: BRG1, *SMARCA4,* chromatin remodelling, cancer, gene expression, cell cycle, transcription, DNA replication

BACKGROUND

Nucleosomes serve as a physical backbone for chromatin organization on a global scale and at local gene regulatory elements. Nucleosomes therefore govern both genome-wide stability and local DNA accessibility (1). Nucleosome positioning by ATP-dependent chromatin remodellers plays a critical role in regulating DNA accessibility and allows genes to be expressed at the appropriate place and time (1). Genomic profiling has demonstrated that dynamic regulation of DNA accessibility occurs primarily at DNA regulatory elements, which are cell type specific, and that DNA accessibility changes reflect concomitant transcriptional patterns. (2, 3). It is essential for chromatin to be relaxed at active gene promoters to create an ordered nucleosome disassembly, which permits binding of RNA pol II and the general transcription machinery (4, 5). In agreement, ChIP-seq data show that transcription factors are concentrated on accessible DNA, with the highest levels of bound transcription factors correlating with the most accessible genomic regions (6). Conversely, chromatin condensation resulting in reduced DNA accessibility is necessary for transcriptional repression (7). Disruption to the DNA accessibility landscape is a feature of cancer (2, 8, 9). This was recently emphasized in genomic sequencing data from multiple cancers and cancer subtypes, which revealed associations between the accessible chromatin organization and mutation load (8). Moreover, studies of aged human and yeast cells demonstrated that nucleosome loss compromises genome stability, gene regulation and transcription (10, 11).

Genes encoding ATP-dependent chromatin remodellers are themselves frequently mutated and often atypically expressed in cancer (5, 12-16). Notably, the SWI/SNF chromatin remodelling complex is mutated or transcriptionally deregulated in ~20% of cancers; a mutation frequency approaching that of *TP53* (~26%) (12, 14, 17). The SWI/SNF complex is often described as a tumour suppressor because it is required by the Retinoblastoma protein (Rb) family for regulation of normal cell growth (18, 19). Disruptions of multiple SWI/SNF subunits are reported in human

tumours and cell lines (13-15, 20-37), often accompanied by a loss of heterozygosity consistent with the inactivation of a tumour suppressor (13, 34). The specific SWI/SNF mutations observed in tumours and the cancers associated with altered SWI/SNF function have been extensively reviewed (12-15, 26, 31, 34, 38). However, the mechanism and functional consequences of SWI/SNF dysregulation are still being defined.

Brahma-related gene 1 (BRG1) is one of the two mutually exclusive ATPases within the SWI/SNF complex. Interestingly, *SMARCA4*, the gene encoding BRG1, has been observed in both down- and up- regulated states in cancer, indicative of the diverse and complex BRG1 functions. *SMARCA4* mRNA was seen to be down regulated in bladder, colon, non-triple negative breast cancers, head and neck, oesophageal, melanoma, pancreatic, lung and ovarian cancers, and *SMARCA4* mutation rates in these cancers have been reported between 4-13% (12-14, 22, 24, 30, 39-41). In contrast, *SMARCA4* has been reported as over expressed in cancers of the prostate, triple negative breast cancers and some leukaemias (12, 22, 24, 30, 42, 43). In *SMARCA4* over expressing cancers, no significant recurrent mutations have been reported (42, 44-46). The importance of BRG1 in cancer is further evidenced through studies of synthetic lethality, where BRG1 was observed to have a synthetic lethal relationship with the alternative SWI/SNF ATPase Braham (BRM), and Aurora A kinase in lung cancer, and PTEN in prostate cancer (43, 47, 48).

Examination of multiple prostate cancer cohorts has demonstrated elevated *SMARCA4* expression or increased BRG1 protein levels. Clinical studies of primary prostate tumours reported an overall increase in BRG1 protein by immunohistochemistry (42, 44-46). Moreover, increased *SMARCA4* gene expression has been reported in tumours from The Cancer Genome Atlas (TCGA) prostate cancer cohort (49, 50). While it is established that BRG1 is commonly up regulated in prostate cancer, the full range of molecular pathways impacted by dysregulated BRG1 levels and the contribution of these molecular changes to the atypical phenotype of prostate cancer cells remains

unclear.

BRG1 has known roles in regulating DNA for temporal gene expression at both promoters and enhancer gene regulatory elements (4, 51-56). Moreover, BRG1 maintains the epigenetic landscape of a cell at these gene regulatory elements. Specifically, BRG1 has been directly linked to transcriptional output through its recognition of H3K14ac (57-59). In the absence of H3K14ac, BRG1 is still present at promoters and histones are disassembled from the chromatin; however, transcription is reduced (60). At enhancers, BRG1 depletion greatly reduces H3K27ac and subtlety reduces H3K4me1, which is correlated with a decrease in chromatin accessibility (53). BRG1 is also known to mediate inter-chromosomal looping interactions between specific loci such as the *MYC* enhancer and promoter, the alpha-globulin genes, the *IgH* locus, and the class II major histocompatibility complex gene locus (24, 61-64). On a global scale, BRG1 binding has been found at DNA-loop anchors (56) and topological associated domain (TAD) boundaries where it increases their stability (65). Together, this demonstrates an important role for BRG1 in maintaining chromatin architecture at both local and global levels for transcription regulation.

Here we dissected the molecular role of BRG1 on the transcriptome in prostate cancer. We confirmed that *SMARCA4* is over-expressed in prostate cancer irrespective of severity or cancer subtype and identified *SMARCA4* was also over expressed in a panel of prostate cancer cell lines. Depletion of BRG1 in LNCaP prostate cancer cells resulted in a modest effect on global gene transcription with most changes resulting in down-regulated gene expression. Within the cohort of down-regulated genes in BRG1 depleted cells we identified gene clusters defined by their co-occupancy or independence from transcription factors AR and FOXA1, both of which are known BRG1 co-activators (66-68). Our data revealed that BRG1, AR and FOXA1 co-regulate known prostate cancer genes *KLK2*, *PCAT1* and *VAV3*. Gene ontology analysis further revealed that genes regulated by BRG1 independent of AR and FOXA1 include factors regulating cell cycle and

proliferation processes including DNA replication. In agreement, depleting BRG1 promoted G1 arrest resulting in reduced cell proliferation. Cumulatively the data indicate BRG1 promotes expression of cellular proliferation factors and cancer-associated genes in prostate cancer cells.

RESULTS

SMARCA4 is over expressed in prostate cancer irrespective of tumour grade or subtype

We first examined the expression of *SMARCA4* in the TCGA (50) prostate normal and cancer cohort. The 486 tumour samples were subset into the seven TCGA categorised molecular subtypes of prostate cancer (50). These included those with fusion genes involving *ERG* (46%), *ETV1* (8%), *ETV4* (4%) and *FLI1* (1%), or those with mutations in *SPOP* (11%), *FOXA1* (3%) or *IDH1* (1%) (50). The remaining samples were grouped as 'other' (26%). Each subtype exhibited a statistically significant increase in *SMARCA4* expression ($p<0.05$) with the exception of the 'FLI1' subtype ($p=0.5899$) and 'other' ($p=0.1899$), which both demonstrated a non-significant increase in *SMARCA4* expression (Figure 1A). Previous work examining *SMARCA4* expression in the TCGA prostate cancer cohort demonstrated that it is also up-regulated irrespective of Gleason score (49). Therefore, we conclude that at the mRNA level, *SMARCA4* is universally over-expressed in prostate cancer, regardless of clinical grade or molecular subtype.

SMARCA4 is over expressed in prostate cancer and transformed prostate cell lines

We next examined both BRG1 protein and *SMARCA4* gene expression levels in normal prostate epithelial cells (PrEC) and compared to LNCaP (lymph node metastasis), an androgen-dependent prostate cancer cell line, as well as PC3 (bone metastasis), an androgen-independent prostate cancer cell line. We found that *SMARCA4* gene expression was increased ~9 fold in LNCaP cells and ~6 fold in PC3 compared to PrEC ($p<0.001$; Figure 1B). Further, the BRG1 protein level was increased ~20 and ~24 fold, respectively, in each of the prostate cancer cell lines compared to

PrEC (Figure 1C). We compared this to published RNA-seq data of several normal, cancer and transformed prostate cell lines (69). The mean expression of *SMARCA4* was significantly increased in both the cancer cell lines and the transformed cell lines compared to the normal cells ($p=0.0148$ and $p=0.0353$ respectively; Figure 1D). The exception was DU145 cells that has a known frameshift mutation in *SMARCA4,* resulting in reduced expression (36). This data show that common prostate cancer cell lines reflect the same pattern of increased BRG1 protein that is observed in prostate tumours compared to normal prostate samples and therefore provides an appropriate model system to explore the functional consequences of BRG1 dysregulation on the transcriptome.

BRG1 is required for the maintenance of active gene expression

Our previous work has shown that BRG1 occupancy is enriched at active promoter and enhancer gene regulatory elements in LNCaP cells (56). We therefore hypothesised that BRG1 would play an important role in maintaining the transcriptional profile of these cells. To assess this, we depleted the level of BRG1 protein using two independent siRNAs targeting *SMARCA4* (si-*SMARCA4*-1 and si-*SMARCA4*-2) and performed RNA-seq at 72 and 144 hours post transfection (Figure 2A). Initial assessment of our RNA-seq data confirmed successful depletion of the *SMARCA4* transcript (~80%) at both time points (Figure 2B). Additionally, we confirmed substantial depletion of BRG1 levels reduced to ~40% of the non-targeting control at 72 hours, and to ~20% of the non-targeting control at 144 hours post-transfection (Figure 2C). We note there were no significant changes detected in the gene expression of any other SWI/SNF subunit proteins (Supplementary Figure 1A). Further quality assessment of the RNA-seq data through a principal component analysis demonstrated that the samples separated by time-point on the first dimension, accounting for 43.39 % of the sample variance (Supplementary Figure 1B). We performed a differential gene expression analysis and identified 169 down-regulated genes and 24 up-regulated genes ($logFC > 1.5$, $FDR < 0.05$) at 72 hours post BRG1 depletion (Figure 2D). This increased to

183 800 down-regulated genes and 174 up-regulated genes by 144 hours post-transfection (Figure 2E).
184 This suggests that the primary role of BRG1 in LNCaP cells is to maintain active gene expression
185 of a subset of genes.
186
187 **BRG1 does not function in the regulation of alternative splicing**
188 The nucleosome barrier within genes is reported to contribute to alternative splicing, where there
189 is a higher conservation of nucleosomes at the splice sites of constitutive exons compared to
190 skipped exons (70-72). Since the contribution of BRG1 to alternative splicing regulation is
191 unknown, we investigated if alterations in alternative splicing may explain down regulation of
192 gene expression after BRG1 depletion in LNCaP cells. To do this we performed a multivariate
193 analysis of transcript splicing (MATS; (73-75)) of our RNA-seq datasets. After 72 hours of BRG1
194 depletion, MATS pairwise comparison detected a genome wide total of 13 and 11 skipped exons,
195 and 14 and 9 retained introns with si-*SMARCA4*-1 and si-*SMARCA4*-2 respectively
196 (Supplementary Figure 1C). At 144 hours post BRG1 knockdown this increased to 240 and 260
197 skipped exons, and 27 and 26 retained introns with si-*SMARCA4*-1 and si-*SMARCA4*-2,
198 respectively (Supplementary Figure 1D). Given the relatively large number of intron-exon
199 junctions within the total LNCaP transcriptome, we conclude BRG1 does not extensively
200 contribute to alternative splicing as the mechanism for predominant gene down-regulation.
201 However, we do note that at 144 hours post-knockdown the MATS analysis identified retention
202 of the first intron from the Kallikrein 3 gene, which encodes prostate specific antigen (PSA)
203 (Supplementary Figure 1E). This splice variant has previously been reported in LNCaP cells and
204 generates a unique protein from canonical PSA (76). While PSA has a well-known link to prostate
205 cancer, the function of its alternative splice variant remains unknown.
206
207 **BRG1 binding is associated with expression of prostate cancer associated genes**
208 We further examined our RNA-seq datasets to determine which genes showed a significant change

209 in expression at 72 hours that was maintained at 144 hours. Of the genes that were down-regulated
210 at the 72 hour time point, 126 genes (75 %) remained down-regulated at 144 hours. Similarly, of
211 the up-regulated genes, 16 (67 %) remained up-regulated at the extended time point (Figure 3A).
212 Within the down-regulated gene set we note a number of genes that have previously been
213 associated with increased proliferation in prostate cancer; these include kallikrein 2 (*KLK2*), long
214 non-coding RNA prostate cancer associated transcript 1 (*PCAT1*), Vav guanine nucleotide
215 exchange factor 3 (*VAV3*) (69, 77-84) (Figure 3B-D). We also examined the panel of prostate cell
216 lines (69) and confirmed that, on average there is elevated expression of these genes in both
217 prostate cancer cells and transformed prostate cell lines compared to normal prostate cells
218 (Supplementary Figure 2A). This suggests a role for BRG1 in maintaining the expression of genes
219 associated with prostate cancer proliferation.
220
221 We next sought to further explore commonalities in the genes with a significant change in
222 expression at both time points. We used 'Enrichr' (85, 86) to determine which existing ChIP-seq
223 datasets of transcription factors had enriched binding at the promoters of these genes. We
224 discovered that the most significantly enriched datasets were for the androgen receptor (AR) and
225 Forkhead box A1 (FOXA1) (Figure 3E), both of which are important for prostate cancer growth
226 (66, 67, 87-91). To investigate the potential coordinated function of these transcription factors with
227 BRG1, we compare the ChIP-seq signal of BRG1 (91), AR (87) and FOXA1 (87) at BRG1
228 genome-wide binding sites in LNCaP cells. We found the profiles separated into three clusters.
229 Cluster 1 sites displayed strong AR and FOXA1 binding, cluster 2 had moderate AR and strong
230 FOXA1, and cluster 3 had minimal to no signal for AR or FOXA1 (Figure 3F). We next examined
231 the key BRG1 regulated genes *KLK2*, *PCAT1* and *VAV3*, and found coordinated binding of all
232 three factors at the promoters of *KLK2* and *PCAT1*, and binding of BRG1 and FOXA1 upstream
233 of the internal 3-prime promoter of *VAV3* (Figure 3G). Furthermore, we showed that the expression
234 of AR or FOXA1 themselves was not regulated by BRG1 (Supplementary Figure 2B-C),

suggesting that the loss of BRG1 is enough to disrupt expression and regulation of *KLK2*, *PCAT1* and *VAV3*.

BRG1 binding is associated with the expression of DNA replication genes

As the majority of significant gene changes occurred at 144 hours post-knockdown, we next investigated potential gene regulatory networks. Gene ontology analysis with Enrichr (85, 86) identified several significant (FDR < 0.05) GO terms pertaining to biological processes, cellular component and molecular function that were all broadly related to the cell cycle (Figure 4A). As BRG1 has previously been shown to interact with cell cycle master regulators, such as Rb and p53 (19, 92-94), we explored the relationship between the cell cycle and BRG1 further in our datasets. We compiled a list of 250 genes related to cell cycle processes, curated from the cell cycle GO terms, and of these examined the top 40 most significantly down-regulated genes in our dataset. Of note among the list were several key genes involved in DNA replication initiation such as *CDC6*, *CDT1* and *CDC45*, as well as the Minichromosome Maintenance (MCM) replicative helicase components *MCM2* and *MCM5* (Figure 4B). To investigate if the effect on replication initiation gene expression was more widespread, we reviewed the gene expression of the other components in the MCM2-7 replicative helicase and the Origin Recognition Complex (ORC) and found that several of these genes were also down-regulated (Figure 4C-D). We confirmed the down regulation of MCM5, CDC6 and ORC6 via Western blot, along with cell cycle regulator CHK1, which revealed almost undetectable expression by 144 hours post BRG1 knockdown (Figure 4E-F).

We investigated whether AR and FOXA1 were also colocalised with BRG1 at DNA replication genes. We examined the ChIP-seq binding profiles of AR, FOXA1 and BRG1 at the promoters of 91 DNA replication genes (determined from the DNA replication GO terms) that were expressed in LNCaP cells. We found at promoters of these genes containing the active histone marks

H3K4me3 and H3K27ac, also displayed a weak BRG1 ChIP-seq signal, but were completely absent of AR and FOXA1 ChIP-seq peaks (Supplementary Figure 3A), for example at the promoters of *CDC45*, *ORC6* (Supplementary Figure 3B). Additionally, we also note this pattern at a putative enhancer region within the *MCM2* gene (Supplementary Figure 3B). Our data suggests that BRG1 binding is associated with the expression of DNA replication genes in prostate cancer cells that is independent of AR and FOXA1.

BRG1 depletion arrests cells in G1

Given BRG1 regulates several genes involved in proliferation and replication, we next asked if BRG1 depletion would alter cell cycle progression in LNCaP cells. We investigated this utilising the same siRNA-mediated approach to target BRG1 by depleting *SMARCA4* and conducted flow cytometry cell cycle analysis at 72 and 144 hours post knockdown. We detected an increase of cells in G1 at 72 hours, which was enhanced by 144 hours. Specifically, at 144 hours post BRG1 depletion there was ~20% increase of cells in G1 and equivalent loss of cells in S phase (Figure 4G-H). These data suggest that a loss of BRG1 reduces proliferation through mediating a G1 arrest.

DISCUSSION

Here we examined the involvement of the SWI/SNF chromatin remodeller BRG1 and its associated encoding gene *SMARCA4* in prostate cancer transcriptional deregulation. We found that over expression of *SMARCA4* commonly occurs in both the TCGA prostate cancer cohort, irrespective of tumour subtype, and in a panel of prostate cancer cell lines. We also found that knockdown of the *SMARCA4* gene, and consequently the BRG1 protein, results in down-regulation of pro-proliferative transcriptional pathways. These included genes already known to promote prostate cancer proliferation, as well as cell cycle and DNA replication genes. Reduction of gene expression in these pathways was concomitant with G1 arrest. Taken together, our results

provide new insights into BRG1's contribution to transcriptional patterns relating to proliferation in prostate cancer.

We have demonstrated that *SMARCA4* mRNA over expression is a universal feature of prostate cancer. Clinical datasets have shown BRG1 protein levels are over-expressed in prostate cancer, in the absence of consistent significant deleterious genetic mutations evident in *SMARCA4* (42, 44-46). Using the large prostate cancer cohort from TCGA (50) we found that *SMARCA4* was significantly over-expressed. Consistent with this, *SMARCA4* expression was increased in a panel of both prostate cancer and transformed cell lines. These data emphasise that the overall increased expression of *SMARCA4* is a characteristic of prostate cancer, irrespective of subtype.

BRG1 depletion followed by RNA-seq revealed multiple transcriptomic alterations that were regulated by BRG1 and related to proliferation. BRG1 depletion primarily resulted in the down-regulation of BRG1's target genes, indicating the main role of BRG1 is to promote active gene expression. Within the down-regulated genes were genes associated with increased proliferation in prostate cancer including *KLK2*, *PCAT-1* and *VAV3*. KLK2 is a known activator of PSA, which is an important biomarker of prostate cancer, and associated with decreased apoptosis (77, 84). *PCAT-1* promotes proliferation through the oncoprotein Myc (69, 81), while VAV3 regulates AR activity to stimulate growth in prostate cancer (78-80, 82). Both *PCAT-1* and VAV3 are correlated with disease progression. Through an analysis of gene ontologies, we also found several cell cycle gene pathways were downregulated with BRG1 depletion. This included numerous genes involved in DNA replication, which were among the most significantly down regulated genes following BRG1 depletion. BRG1 is known to have a role in driving self-renewal and malignancy in B-cell acute lymphoblastic and acute myeloid leukaemias, cancers which also have over expressed BRG1 (22, 24). Specifically, these leukaemias require high levels of BRG1 for de-condensation of the cell specific *MYC* enhancer. In these cancers, a loss of BRG1 causes a reduction of enhancer-

313 promoter interactions, reduced transcription factor occupancy and DNA looping which in turn
314 reduces *MYC* expression (24). This implies that the overexpression of BRG1 contributes to driving
315 oncogenic transcriptional programs which influence the proliferation capacity of cancer cells.
316
317 Our data revealed that BRG1 co-occupied the promotors of proliferation associated genes (*KLK2*,
318 *PCAT-1* and *VAV3)* along with AR and FOXA1, and that these genes were down-regulated across
319 our experimental time course. Co-regulation of transcription by AR and FOXA1 in prostate cancer
320 is associated with reprogrammed binding of AR and oncogenic patterns of gene expression that
321 are essential for AR-driven proliferation (95, 96). Additionally, there is a high overlap of these
322 reprogrammed AR binding sites between LNCaP cells and primary prostate tumour tissue (96).
323 Here we have shown BRG1 gene regulation overlaps with these transcription factors at gene
324 promoters, which is concomitant with expression of prostate cancer associated genes. However, it
325 is noteworthy that BRG1 depletion also altered the expression of DNA replication genes through
326 a mechanism that appears independent of AR and FOXA1. This data suggests that BRG1 has
327 additional roles in other gene regulatory networks, which may indirectly influence cell
328 proliferation. As BRG1 is known to interact with cell cycle regulators in other cancers, it is
329 possible that genes co-regulated by BRG1, AR and FOXA1 are important in a prostate cancer
330 context, while regulation of cell cycle and DNA replication genes may be a general feature of
331 BRG1 over expression in cancer.
332
333 **CONCLUSIONS**
334
335 In summary, our data identifies fundamental role for BRG1 in maintaining active transcription for
336 proliferation of prostate cancer cells. We find that BRG1 promotes gene expression in prostate
337 cancer models with varying degrees of dependence on AR and FOXA1. BRG1 is required to drive
338 the expression of numerous prostate cancer specific genes in an AR/FOXA1 dependant manner,

but also works independently to drive the expression of pro-proliferative and DNA replication genes. These results provide important functional information regarding the role of BRG1 controlling proliferation in prostate cancer cells.

METHODS

Cell Culture and siRNA Transfection

Normal Prostate Epithelial Cells (PrEC) cells (Cambrex Bio Science, #CC-2555) were cultured in PrEBM (Clonetics, #CC-3165) according to the manufacturer's protocol. Briefly, PrEC cells were seeded at 2,500 cells per cm^2 and medium was replaced every two days. Cells were passaged at approximately 80 % confluence. To passage a T75 flask, PrEC cells were rinsed in 6 mls Hanks Balanced Salt Solution (Thermo Fisher Scientific, #14025076) then detached with 2 ml pre-warmed 0.025 % Trypsin-EDTA and incubated at room temperature for 5 minutes. Trypsin was inactivated with 12 mls of Trypsin-Neutralizing Solution (Clonetics, #CC-5002) and cells were centrifuged at 300 x g for 5 minutes. The supernatant was aspirated, and the cell pellet was re-suspended in PrEBM. The number of cells was determined on the Countess automated counter and were re-seeded at the appropriate density based on experimental needs. Cells were discarded after ~16 population doublings.

PC3 cells (ATCC, #CRL-1435) were maintained in RPMI medium (Gibco, #11875-093) with 10 % FBS, 11 mls of 1 M HEPES (Gibco, #15630080) and Pen/Strep. LNCaP cells (ATCC, #CRL-1740) were cultured using custom T-Medium from Gibco (DMEM low glucose (GIBCO cat# 31600-034), Kaighn's modified F-12 medium (F-12K; cat# 211227-014), insulin 500x bovine pancreas (Sigma cat# I1882.10MG), T3 6.825 ng/ml Tri-iodothyronine (Sigma cat# T5516), Transferrin 500x (Sigma cat# T5391), Biotin 500x (Sigma cat# B4639), Adenine 500x (Sigma cat# A3259)). Both prostate cell lines were cultured under recommend conditions; 37ºC with 5 %

365 CO_2. When the cells reached ~80 % confluence they were passaged or seeded as per experimental
366 requirements. For siRNA transfection LNCaP cells were seeded into 6-well plates at a density of
367 2.5 x 10^5 cells per well or 10cm dishes at 1.5 x 10^6 cells per dish. The cells were transfected with
368 either on target *SMARCA4* siRNA (Horizon, #J-010431-06-0005 or #J-010431-07-0005) or the
369 non-targeting control siRNA pool (Horizon, #D-001810-10-05) 24 hours after seeding the cells
370 using DharmaFECT 2 (Thermo Scientific, #T-2002-03) as per the manufacturer's instructions. To
371 maintain the knockdown over a 6-day period, at 72 hours post transfection the cells were harvested,
372 split at a ratio of 1:2 into two new wells, and reverse-transfected with siRNA. The cells were then
373 incubated for a further 72 hours before collection.
374
375 ***Quantitative Real-Time PCR (qRT-PCR)***
376 RNA was extracted with TRIzol reagent (Thermo Scientific, #15596026), according to the
377 manufacturer's protocol. Extracted RNA was re-suspended in 30 ul of nuclease-free water and
378 quantified on the NanoDrop spectrophotometer (Thermo Scientific). cDNA synthesis was carried
379 out with 500 ng of RNA using the SensiFAST cDNA Synthesis Kit (Bioline, #BIO-65054)
380 according to the manufacturer's instructions.
381
382 qRT-PCR was carried out on the CFX384 Touch Real-Time PCR Detection System (Bio-Rad). A
383 master mix was made for each qRT-PCR target containing 5 ul of KAPA Universal SYBR Fast
384 PCR mix (KAPA Biosystems, #KK4602), 0.6ul of 5 uM forward primer, 0.6 ul of 5 uM reverse
385 primer and 1.8 ul of nuclease free water per reaction. Reactions conditions were 95ºC for 3
386 minutes, followed by 45x cycles of 95 ºC for 3 seconds and 60 ºC for 30 seconds, then a melt
387 curve analysis (65 ºC to 95 ºC, increasing at a rate of 0.5 ºC every 5secs). Primers to detect
388 *SMARCA4* were CAGAACGCACAGACCTTCAA (forward) and
389 TCACTCTCCTCGCCTTCACT (reverse) and for detection of *18S*
390 GGGACTTAATCAACGCAAGC (forward) and GCAATTATTCCCCATGAACG (reverse).

Relative gene expression was calculated using ddCt and normalised to *18S*. A significant change in gene expression of *SMARCA4* between PrEC, LNCaP and PC3 cells was determined by one-way ANOVA and corrected with Tukey's test for multiple comparisons.

Western Blot

Whole cell lysates were collected with lysis buffer (50 mM HEPES, 150 mM NaCl, 10% Glycerol, 1 % Triton-X-100, 1.5 mM $MgCl_2$, 1 mM EGTA, 10 mM Pyrophosphate, 100 mM NaF, Roche protease inhibitor cocktail 1x), and protein level quantified using the Pierce BCA Assay Kit (Thermo Scientific, #23227) according to the manufacturer's instructions. Sample reducing agent (Thermo Scientific, NP0004), loading buffer (Thermo Scientific, NP0007) and 10 ug protein were combined with water to a final volume of 25 ul. Protein samples were heated at 90 ºC for 5 minutes then allowed to cool to room temperature. Protein samples were loaded on a NuPage Novex Bis-Tris 4-12 % gel (Thermo Scientific, NP0321BOX) and electrophoresed at 100V for 1.5 hours in a 1x MOPS buffer (50 mM MOPS (Biochemicals Astral Scientific, #BIOMB03600, 50 mM Tris base, 0.1% SDS, 1 mM EDTA [pH 7.7]). Proteins were transferred to a polyvinylidene fluoride membrane (Bio-Rad, #1620177) at 30 volts for 1 hour using 1x transfer buffer (25 mM Tris base, 192 mM Glycine [pH 8.3]) with 10 % methanol (Sigma-Aldrich, #322415). Membranes were blocked for 1 hour with 5 % skim milk in TBS-T (20 mM Tris, 150 mM NaCl, 0.1% Tween 20 [pH 7.6]) at 4ºC. Primary antibodies used were BRG1 (Santa Cruz, sc-10768X), GAPDH (Ambion, AM4300), CHK1 (CST, 2360S), ORC6 (CST, 4737S), CDC6 (CST, 3387S) and MCM5 (abcam, ab17967). Primary antibodies were incubated on samples overnight at 4 ºC with rotation. The membrane was then washed three times for 10mins each in TBS-T with rotation. Secondary antibodies goat anti-mouse (Santa Cruz, sc-2005) and goat anti-rabbit (Santa Cruz, sc-2004) were diluted in TBS-T containing 5 % skim milk and incubated at 4 ºC with rotation for 1 hour. The membrane was washed three times for 10 minutes in TBS-T. The membrane was then covered with ECL solution (Perkin Elmer, #NEL104001EA), incubated for 1min at room temperature, and

visualized by X-ray film. Adjusted relative density calculations were processed through ImageJ (97, 98).

Flow cytometric cell cycle analysis

LNCaP cells were seeded at 1.5 x 10^6 cells per 10 cm dish and transfected with siRNA as described. At 72 and 144 hours post transfection the cells were treated with 10 uM EdU for 30 minutes. Remaining EdU was washed off the cells with PBS before harvesting cells, then 1 x 10^6 cells were fixed in 70 % ethanol and frozen at -20 ºC. Cells were then diluted 1 in 4 with PBS then pelleted and re-suspended in 1 ml of PBS containing 1 % BSA (Sigma-Aldrich, #A2058). Cells were again pelleted, re-suspended in 500 ul of click reaction mix (10uM carbocyfluorescine TEG-azide, 10 mM Sodium L-ascorbate, and 2 mM Copper-II-sulphate diluted in PBS), and incubated in the dark at room temperature for 30 minutes. Samples were then diluted with 5 mls of PBS containing 1 % BSA and 0.1 % Tween-20. Cells were again pelleted, washed with PBS and then resuspended in 500 ul of PBS containing 1% BSA, 0.1 mg/ml of RNase and 1 ug/ml of DAPI. Samples were analyised on the Canto II (BD Biosciences). Forward and side scatter were used to select a population of cells free of cell debris and doublets. Cells were analysed using B450 (FTIC – EdU positive) and B510 (DAPI) lasers. 50,000 single cell events were recorded for each ample. FlowJo software v10.5, was used to analyse the data. Data was collected in biological duplicate.

RNA-seq Experiments

Total RNA was extracted with TRIzol reagent, quantified on the Qubit and quality assessed with the Bioanalyzer. An aliquot of 500 ng of total RNA was spiked with external controls ERCC RNA spike-in Mix (Thermo Scientific, 4456740) and libraries constructed with the TruSeq Stranded mRNA sample preparation kit (Illumina, 20020594) according to the manufacturer's protocol. mRNA Libraries were quantified on Qubit and then stored at -20 ºC. Library quality and fragment size of RNA-seq libraries was assessed on the Bioanalyzer, then KAPA Library Quantification

(KAPA Biosystems, #KK4824) was performed according to the manufacturer's protocol. The KAPA quantification results were used to dilute the libraries to 2 nM for sequencing. RNA-seq samples were sequenced for 100 cycles of paired-end reads on the Illumina HiSeq 2500 platform, with four samples multiplexed per lane of the high output run.

RNA-seq Data Analysis

RNA-seq data was processed as described in Taberlay & Achinger-Kawecka *et al.* (9). Briefly, read counts were normalized with ERCC spike in controls, mapped to hg19/GRCh37 using STAR and counted into genes using the featureCounts (99) program. GENCODE v19 was used as a reference transcriptome to determine the transcript per million read (TPM) value. Fold change was calculated within each time point as the log2 ratio of normalized reads per gene using the *edgeR* package in R. Genes with a fold change of ± 1.5 and FDR < 0.01 were considered significantly different. Volcano plots of differential expression were created in R with *ggplots2* and heatmaps with the *heatmap2* package with normalised row Z-score. PCA was performed in R using the *edgeR* package with log counts per million (logCPMS) over GENCODE v19 annotated gene coordinates and normalizing the read counts to library size. RNA-seq multivariate analysis of transcript splicing (MATS) to calculate exon skipping and intron retention was performed with the MATS python package v4.0.2 (73-75). Transcription factor and GO term enrichment was obtained from Enrichr (http://amp.pharm.mssm.edu/Enrichr/) online gene list analysis tool (85, 86).

TCGA and prostate cell line expression analysis

Pre-processed RNA-seq data from the TCGA prostate adenocarcinoma cohort was downloaded (cancergenome.nih.gov) for both normal and tumour samples. The average of tumour (n = 486) and normal (n = 52) samples was calculated to determine mean expression. Separation of tumours by Gleason score and molecular subtype was performed in R using the associated clinical data to subset the appropriate groups. Significance was calculated for tumour versus normal using an

unpaired T-test. For comparison between Gleason score or molecular subtype, significance was calculated using one-way ANOVA with Dunnett's multiple comparison correction.

Expression data for prostate cell lines from Presner et al. (69) was downloaded from http://www.betastasis.com/prostate_cancer/. Significance between normal, cancer and transformed cell lines was calculated using one-way ANOVA with Dunnett's multiple comparison correction.

ChIP-seq data

The following LNCaP ChIP-seq data was obtained from GEO (ncbi.nlm.nih.gov/geo/); BRG1 accession GSE72690 (91), H3K4me3 and H3K27me3 accession GSE38685 (100), H3K27ac and H3K4me1 accession GSE73785 (9). These data were processed through NGSane pipeline as previously described (9, 100). Pre-processed bigwig files for FOXA1 and AR were obtained from GEO accession GSE114274 (87). Genome browser images of ChIP-seq data were taken from IGV. Heatmaps of ChIP-seq signal were created with *deeptools* (101).

DECLARATIONS

Ethics approval and consent to participate

Not Applicable

Consent for publication

Not Applicable

Availability of data and materials

The BRG1 knockdown RNA-seq data generated for this study has been submitted to GEO, accession number GSE150252. Reviewer access for the submitted data is available from; https://www.ncbi.nlm.nih.gov/geo/query/acc.cgi?acc=GSE150252

Competing interests

The authors declare that they have no competing interests.

Funding

This work is supported by grants awarded to A.J.C, S.J.C and P.C.T. A.J.C. is supported by grants from the NHMRC (1162886, 1185870), the Goodridge Foundation and the Neil and Norma Hill Foundation. S.J.C. is supported by grants (1011447, 1070418, 1051757) and a fellowship (1156408) from the NHMRC. P.C.T. is supported by project grants from the Cure Cancer Australia Foundation (1060713) and the NHMRC (1051757, 1161985), and a fellowship (1109696) and investigator grant from the NHMRC (1176417).

Authors' contributions

This study was initiated and deisgned by KAG, SJC and PCT. Experiments were performed by KAG, SGP and GK. Analysis and interpretation of next-generation data was performed by KAG, CMG, JAK and PL. Initial manuscript draft was written by KAG. Manuscript editing and reviewing was conducted by KAG, JAK, SGP, GK, AJC, SJC and PCT. All authors have read and approval the final version of this manuscript. Funding for this work was provided by AJC, SJC and PCT.

Acknowledgements

We thank Suat Dervish and the Westmead Flow Cytometry facility for the FACS analysis infrastructure.

REFERENCES

1. Giles KA, Taberlay PC. The Role of Nucleosomes in Epigenetic Gene Regulation. Clinical Epigenetics. 2019:87-117.

2. Taberlay PC, Statham AL, Kelly TK, Clark SJ, Jones PA. Reconfiguration of nucleosome-depleted regions at distal regulatory elements accompanies DNA methylation of enhancers and insulators in cancer. Genome Res. 2014;24(9):1421-32.

3. Thurman RE, Rynes E, Humbert R, Vierstra J, Maurano MT, Haugen E, et al. The accessible chromatin landscape of the human genome. Nature. 2012;489(7414):75-82.

4. Heintzman ND, Stuart RK, Hon G, Fu Y, Ching CW, Hawkins RD, et al. Distinct and predictive chromatin signatures of transcriptional promoters and enhancers in the human genome. Nat Genet. 2007;39(3):311-8.

5. Skulte KA, Phan L, Clark SJ, Taberlay PC. Chromatin remodeler mutations in human cancers: epigenetic implications. Epigenomics. 2014;6(4):397-414.

6. Li XY, Thomas S, Sabo PJ, Eisen MB, Stamatoyannopoulos JA, Biggin MD. The role of chromatin accessibility in directing the widespread, overlapping patterns of Drosophila transcription factor binding. Genome Biol. 2011;12(4):R34.

7. Venkatesh S, Workman JL. Histone exchange, chromatin structure and the regulation of transcription. Nature reviews Molecular cell biology. 2015;16(3):178-89.

8. Makova KD, Hardison RC. The effects of chromatin organization on variation in mutation rates in the genome. Nat Rev Genet. 2015;16(4):213-23.

9. Taberlay PC, Achinger-Kawecka J, Lun AT, Buske FA, Sabir K, Gould CM, et al. Three-dimensional disorganization of the cancer genome occurs coincident with long-range genetic and epigenetic alterations. Genome Res. 2016;26(6):719-31.

10. Hu Z, Chen K, Xia Z, Chavez M, Pal S, Seol JH, et al. Nucleosome loss leads to global transcriptional up-regulation and genomic instability during yeast aging. Genes Dev. 2014;28(4):396-408.

11. O'Sullivan RJ, Kubicek S, Schreiber SL, Karlseder J. Reduced histone biosynthesis and chromatin changes arising from a damage signal at telomeres. Nat Struct Mol Biol. 2010;17(10):1218-25.

12. Giles KA, Taberlay PC. Mutations in Chromatin Remodeling Factors. Encyclopedia of Cancer (Third Edition). 2019:511-27.

13. Reisman D, Glaros S, Thompson EA. The SWI/SNF complex and cancer. Oncogene. 2009;28(14):1653-68.

14. Shain AH, Pollack JR. The spectrum of SWI/SNF mutations, ubiquitous in human cancers. PLoS One. 2013;8(1):e55119.

15. Wilson BG, Roberts CW. SWI/SNF nucleosome remodellers and cancer. Nat Rev Cancer. 2011;11(7):481-92.

16. Chu X, Guo X, Jiang Y, Yu H, Liu L, Shan W, et al. Genotranscriptomic meta-analysis of the CHD family chromatin remodelers in human cancers - initial evidence of an oncogenic role for CHD7. Mol Oncol. 2017;11(10):1348-60.

17. Kadoch C, Hargreaves DC, Hodges C, Elias L, Ho L, Ranish J, et al. Proteomic and bioinformatic analysis of mammalian SWI/SNF complexes identifies extensive roles in human malignancy. Nat Genet. 2013;45(6):592-601.

18. Dunaief JL, Strober BE, Guha S, Khavari PA, Alin K, Luban J, et al. The retinoblastoma protein and BRG1 form a complex and cooperate to induce cell cycle arrest. Cell. 1994;79(1):119-30.

19. Strober BE, Dunaief JL, Guha, Goff SP. Functional interactions between the hBRM/hBRG1 transcriptional activators and the pRB family of proteins. Mol Cell Biol. 1996;16(4):1576-83.

571 20. Yokoyama Y, Matsushita Y, Shigeto T, Futagami M, Mizunuma H. Decreased ARID1A
572 expression is correlated with chemoresistance in epithelial ovarian cancer. Journal of
573 gynecologic oncology. 2014;25(1):58-63.
574 21. Song S, Walter V, Karaca M, Li Y, Bartlett CS, Smiraglia DJ, et al. Gene Silencing
575 Associated with SWI/SNF Complex Loss During NSCLC Development. Molecular cancer
576 research : MCR. 2014.
577 22. Buscarlet M, Krasteva V, Ho L, Simon C, Hebert J, Wilhelm B, et al. Essential role of
578 BRG, the ATPase subunit of BAF chromatin remodeling complexes, in leukemia maintenance.
579 Blood. 2014.
580 23. Yan HB, Wang XF, Zhang Q, Tang ZQ, Jiang YH, Fan HZ, et al. Reduced expression of
581 the chromatin remodeling gene ARID1A enhances gastric cancer cell migration and invasion via
582 downregulation of E-cadherin transcription. Carcinogenesis. 2013.
583 24. Shi J, Whyte WA, Zepeda-Mendoza CJ, Milazzo JP, Shen C, Roe JS, et al. Role of
584 SWI/SNF in acute leukemia maintenance and enhancer-mediated Myc regulation. Genes Dev.
585 2013;27(24):2648-62.
586 25. Romero OA, Torres-Diz M, Pros E, Savola S, Gomez A, Moran S, et al. MAX
587 inactivation in small-cell lung cancer disrupts the MYC-SWI/SNF programs and is synthetic
588 lethal with BRG1. Cancer discovery. 2013.
589 26. Oike T, Ogiwara H, Nakano T, Yokota J, Kohno T. Inactivating mutations in SWI/SNF
590 chromatin remodeling genes in human cancer. Jpn J Clin Oncol. 2013;43(9):849-55.
591 27. Mao TL, Ardighieri L, Ayhan A, Kuo KT, Wu CH, Wang TL, et al. Loss of ARID1A
592 expression correlates with stages of tumor progression in uterine endometrioid carcinoma. The
593 American journal of surgical pathology. 2013;37(9):1342-8.
594 28. Cho H, Kim JS, Chung H, Perry C, Lee H, Kim JH. Loss of ARID1A/BAF250a
595 expression is linked to tumor progression and adverse prognosis in cervical cancer. Human
596 pathology. 2013;44(7):1365-74.

29. Bosse T, ter Haar NT, Seeber LM, v Diest PJ, Hes FJ, Vasen HF, et al. Loss of ARID1A expression and its relationship with PI3K-Akt pathway alterations, TP53 and microsatellite instability in endometrial cancer. Modern pathology : an official journal of the United States and Canadian Academy of Pathology, Inc. 2013;26(11):1525-35.

30. Bai J, Mei P, Zhang C, Chen F, Li C, Pan Z, et al. BRG1 is a prognostic marker and potential therapeutic target in human breast cancer. PLoS One. 2013;8(3):e59772.

31. You JS, Jones PA. Cancer genetics and epigenetics: two sides of the same coin? Cancer cell. 2012;22(1):9-20.

32. Katagiri A, Nakayama K, Rahman MT, Rahman M, Katagiri H, Nakayama N, et al. Loss of ARID1A expression is related to shorter progression-free survival and chemoresistance in ovarian clear cell carcinoma. Modern pathology : an official journal of the United States and Canadian Academy of Pathology, Inc. 2012;25(2):282-8.

33. Roberts CW, Biegel JA. The role of SMARCB1/INI1 in development of rhabdoid tumor. Cancer biology & therapy. 2009;8(5):412-6.

34. Roy DM, Walsh LA, Chan TA. Driver mutations of cancer epigenomes. Protein Cell. 2014;5(4):265-96.

35. Zhao J, Liu C, Zhao Z. ARID1A: a potential prognostic factor for breast cancer. Tumour Biol. 2014.

36. Wong AK, Shanahan F, Chen Y, Lian L, Ha P, Hendricks K, et al. BRG1, a component of the SWI-SNF complex, is mutated in multiple human tumor cell lines. Cancer Res. 2000;60(21):6171-7.

37. Medina PP, Romero OA, Kohno T, Montuenga LM, Pio R, Yokota J, et al. Frequent BRG1/SMARCA4-inactivating mutations in human lung cancer cell lines. Hum Mutat. 2008;29(5):617-22.

38. Roberts CW, Orkin SH. The SWI/SNF complex--chromatin and cancer. Nat Rev Cancer. 2004;4(2):133-42.

623 39. Wilson BG, Helming KC, Wang X, Kim Y, Vazquez F, Jagani Z, et al. Residual
624 complexes containing SMARCA2 (BRM) underlie the oncogenic drive of SMARCA4 (BRG1)
625 mutation. Mol Cell Biol. 2014.
626 40. Herpel E, Rieker RJ, Dienemann H, Muley T, Meister M, Hartmann A, et al. SMARCA4
627 and SMARCA2 deficiency in non-small cell lung cancer: immunohistochemical survey of 316
628 consecutive specimens. Ann Diagn Pathol. 2017;26:47-51.
629 41. Agaimy A, Fuchs F, Moskalev EA, Sirbu H, Hartmann A, Haller F. SMARCA4-deficient
630 pulmonary adenocarcinoma: clinicopathological, immunohistochemical, and molecular
631 characteristics of a novel aggressive neoplasm with a consistent TTF1(neg)/CK7(pos)/HepPar-
632 1(pos) immunophenotype. Virchows Arch. 2017;471(5):599-609.
633 42. Sun A, Tawfik O, Gayed B, Thrasher JB, Hoestje S, Li C, et al. Aberrant expression of
634 SWI/SNF catalytic subunits BRG1/BRM is associated with tumor development and increased
635 invasiveness in prostate cancers. Prostate. 2007;67(2):203-13.
636 43. Ding Y, Li N, Dong B, Guo W, Wei H, Chen Q, et al. Chromatin remodeling ATPase
637 BRG1 and PTEN are synthetic lethal in prostate cancer. J Clin Invest. 2019;129(2):759-73.
638 44. Liu XB, Sun AJ, Wang C, Chen LR. [Expression of BRG1 and BRM proteins in prostatic
639 cancer]. Zhonghua Bing Li Xue Za Zhi. 2010;39(9):591-4.
640 45. Li Y, Shi QL, Jin XZ, Meng K, Zhou XJ, Sun LP. [BRG1 expression in prostate
641 carcinoma by application of tissue microarray]. Zhonghua Nan Ke Xue. 2006;12(7):629-32.
642 46. Valdman A, Nordenskjold A, Fang X, Naito A, Al-Shukri S, Larsson C, et al. Mutation
643 analysis of the BRG1 gene in prostate cancer clinical samples. Int J Oncol. 2003;22(5):1003-7.
644 47. Tagal V, Wei S, Zhang W, Brekken RA, Posner BA, Peyton M, et al. SMARCA4-
645 inactivating mutations increase sensitivity to Aurora kinase A inhibitor VX-680 in non-small cell
646 lung cancers. Nat Commun. 2017;8:14098.

647 48. Oike T, Ogiwara H, Tominaga Y, Ito K, Ando O, Tsuta K, et al. A synthetic lethality-
648 based strategy to treat cancers harboring a genetic deficiency in the chromatin remodeling factor
649 BRG1. Cancer Res. 2013;73(17):5508-18.
650 49. Muthuswami R, Bailey L, Rakesh R, Imbalzano AN, Nickerson JA, Hockensmith JW.
651 BRG1 is a prognostic indicator and a potential therapeutic target for prostate cancer. J Cell
652 Physiol. 2019.
653 50. Cancer Genome Atlas Research N. The Molecular Taxonomy of Primary Prostate
654 Cancer. Cell. 2015;163(4):1011-25.
655 51. Tolstorukov MY, Sansam CG, Lu P, Koellhoffer EC, Helming KC, Alver BH, et al.
656 Swi/Snf chromatin remodeling/tumor suppressor complex establishes nucleosome occupancy at
657 target promoters. Proc Natl Acad Sci U S A. 2013;110(25):10165-70.
658 52. Alver BH, Kim KH, Lu P, Wang X, Manchester HE, Wang W, et al. The SWI/SNF
659 chromatin remodelling complex is required for maintenance of lineage specific enhancers. Nat
660 Commun. 2017;8:14648.
661 53. Hodges HC, Stanton BZ, Cermakova K, Chang CY, Miller EL, Kirkland JG, et al.
662 Dominant-negative SMARCA4 mutants alter the accessibility landscape of tissue-unrestricted
663 enhancers. Nat Struct Mol Biol. 2018;25(1):61-72.
664 54. Hu G, Schones DE, Cui K, Ybarra R, Northrup D, Tang Q, et al. Regulation of
665 nucleosome landscape and transcription factor targeting at tissue-specific enhancers by BRG1.
666 Genome Res. 2011;21(10):1650-8.
667 55. Bao X, Rubin AJ, Qu K, Zhang J, Giresi PG, Chang HY, et al. A novel ATAC-seq
668 approach reveals lineage-specific reinforcement of the open chromatin landscape via cooperation
669 between BAF and p63. Genome biology. 2015;16:284.
670 56. Giles KA, Gould CM, Du Q, Skvortsova K, Song JZ, Maddugoda MP, et al. Integrated
671 epigenomic analysis stratifies chromatin remodellers into distinct functional groups. Epigenetics
672 Chromatin. 2019;12(1):12.

673 57. Luebben WR, Sharma N, Nyborg JK. Nucleosome eviction and activated transcription
674 require p300 acetylation of histone H3 lysine 14. Proc Natl Acad Sci U S A.
675 2010;107(45):19254-9.
676 58. Morrison EA, Sanchez JC, Ronan JL, Farrell DP, Varzavand K, Johnson JK, et al. DNA
677 binding drives the association of BRG1/hBRM bromodomains with nucleosomes. Nat Commun.
678 2017;8:16080.
679 59. Shen W, Xu C, Huang W, Zhang J, Carlson JE, Tu X, et al. Solution structure of human
680 Brg1 bromodomain and its specific binding to acetylated histone tails. Biochemistry.
681 2007;46(8):2100-10.
682 60. Church M, Smith KC, Alhussain MM, Pennings S, Fleming AB. Sas3 and Ada2(Gcn5)-
683 dependent histone H3 acetylation is required for transcription elongation at the de-repressed
684 FLO1 gene. Nucleic Acids Res. 2017;45(8):4413-30.
685 61. Kim SI, Bresnick EH, Bultman SJ. BRG1 directly regulates nucleosome structure and
686 chromatin looping of the alpha globin locus to activate transcription. Nucleic Acids Res.
687 2009;37(18):6019-27.
688 62. Kim SI, Bultman SJ, Kiefer CM, Dean A, Bresnick EH. BRG1 requirement for long-
689 range interaction of a locus control region with a downstream promoter. Proc Natl Acad Sci U S
690 A. 2009;106(7):2259-64.
691 63. Bossen C, Murre CS, Chang AN, Mansson R, Rodewald HR, Murre C. The chromatin
692 remodeler Brg1 activates enhancer repertoires to establish B cell identity and modulate cell
693 growth. Nat Immunol. 2015;16(7):775-84.
694 64. Ni Z, Abou El Hassan M, Xu Z, Yu T, Bremner R. The chromatin-remodeling enzyme
695 BRG1 coordinates CIITA induction through many interdependent distal enhancers. Nat
696 Immunol. 2008;9(7):785-93.

697 65. Barutcu AR, Lajoie BR, Fritz AJ, McCord RP, Nickerson JA, van Wijnen AJ, et al.
698 SMARCA4 regulates gene expression and higher-order chromatin structure in proliferating
699 mammary epithelial cells. Genome Res. 2016;26(9):1188-201.
700 66. Dai Y, Ngo D, Jacob J, Forman LW, Faller DV. Prohibitin and the SWI/SNF ATPase
701 subunit BRG1 are required for effective androgen antagonist-mediated transcriptional repression
702 of androgen receptor-regulated genes. Carcinogenesis. 2008;29(9):1725-33.
703 67. Marshall TW, Link KA, Petre-Draviam CE, Knudsen KE. Differential requirement of
704 SWI/SNF for androgen receptor activity. J Biol Chem. 2003;278(33):30605-13.
705 68. Hoffman JA, Trotter KW, Ward JM, Archer TK. BRG1 governs glucocorticoid receptor
706 interactions with chromatin and pioneer factors across the genome. Elife. 2018;7.
707 69. Prensner JR, Iyer MK, Balbin OA, Dhanasekaran SM, Cao Q, Brenner JC, et al.
708 Transcriptome sequencing across a prostate cancer cohort identifies PCAT-1, an unannotated
709 lincRNA implicated in disease progression. Nat Biotechnol. 2011;29(8):742-9.
710 70. Andersson R, Enroth S, Rada-Iglesias A, Wadelius C, Komorowski J. Nucleosomes are
711 well positioned in exons and carry characteristic histone modifications. Genome Res.
712 2009;19(10):1732-41.
713 71. Dhami P, Saffrey P, Bruce AW, Dillon SC, Chiang K, Bonhoure N, et al. Complex exon-
714 intron marking by histone modifications is not determined solely by nucleosome distribution.
715 PLoS One. 2010;5(8):e12339.
716 72. Huang H, Yu S, Liu H, Sun X. Nucleosome organization in sequences of alternative
717 events in human genome. Bio Systems. 2012;109(2):214-9.
718 73. Shen S, Park JW, Huang J, Dittmar KA, Lu ZX, Zhou Q, et al. MATS: a Bayesian
719 framework for flexible detection of differential alternative splicing from RNA-Seq data. Nucleic
720 Acids Res. 2012;40(8):e61.

721 74. Shen S, Park JW, Lu ZX, Lin L, Henry MD, Wu YN, et al. rMATS: robust and flexible
722 detection of differential alternative splicing from replicate RNA-Seq data. Proc Natl Acad Sci U
723 S A. 2014;111(51):E5593-601.
724 75. Park JW, Tokheim C, Shen S, Xing Y. Identifying differential alternative splicing events
725 from RNA sequencing data using RNASeq-MATS. Methods Mol Biol. 2013;1038:171-9.
726 76. David A, Mabjeesh N, Azar I, Biton S, Engel S, Bernstein J, et al. Unusual alternative
727 splicing within the human kallikrein genes KLK2 and KLK3 gives rise to novel prostate-specific
728 proteins. J Biol Chem. 2002;277(20):18084-90.
729 77. Shang Z, Niu Y, Cai Q, Chen J, Tian J, Yeh S, et al. Human kallikrein 2 (KLK2)
730 promotes prostate cancer cell growth via function as a modulator to promote the ARA70-
731 enhanced androgen receptor transactivation. Tumour Biol. 2014;35(3):1881-90.
732 78. Lin KT, Gong J, Li CF, Jang TH, Chen WL, Chen HJ, et al. Vav3-rac1 signaling
733 regulates prostate cancer metastasis with elevated Vav3 expression correlating with prostate
734 cancer progression and posttreatment recurrence. Cancer Res. 2012;72(12):3000-9.
735 79. Liu Y, Mo JQ, Hu Q, Boivin G, Levin L, Lu S, et al. Targeted overexpression of vav3
736 oncogene in prostatic epithelium induces nonbacterial prostatitis and prostate cancer. Cancer
737 Res. 2008;68(15):6396-406.
738 80. Lyons LS, Burnstein KL. Vav3, a Rho GTPase guanine nucleotide exchange factor,
739 increases during progression to androgen independence in prostate cancer cells and potentiates
740 androgen receptor transcriptional activity. Mol Endocrinol. 2006;20(5):1061-72.
741 81. Prensner JR, Chen W, Han S, Iyer MK, Cao Q, Kothari V, et al. The long non-coding
742 RNA PCAT-1 promotes prostate cancer cell proliferation through cMyc. Neoplasia.
743 2014;16(11):900-8.
744 82. Rao S, Lyons LS, Fahrenholtz CD, Wu F, Farooq A, Balkan W, et al. A novel nuclear
745 role for the Vav3 nucleotide exchange factor in androgen receptor coactivation in prostate
746 cancer. Oncogene. 2012;31(6):716-27.

747 83. Shang Z, Yu J, Sun L, Tian J, Zhu S, Zhang B, et al. LncRNA PCAT1 activates AKT and
748 NF-kappaB signaling in castration-resistant prostate cancer by regulating the
749 PHLPP/FKBP51/IKKalpha complex. Nucleic Acids Res. 2019;47(8):4211-25.
750 84. Williams SA, Xu Y, De Marzo AM, Isaacs JT, Denmeade SR. Prostate-specific antigen
751 (PSA) is activated by KLK2 in prostate cancer ex vivo models and in prostate-targeted
752 PSA/KLK2 double transgenic mice. Prostate. 2010;70(7):788-96.
753 85. Chen EY, Tan CM, Kou Y, Duan Q, Wang Z, Meirelles GV, et al. Enrichr: interactive
754 and collaborative HTML5 gene list enrichment analysis tool. BMC Bioinformatics. 2013;14:128.
755 86. Kuleshov MV, Jones MR, Rouillard AD, Fernandez NF, Duan Q, Wang Z, et al. Enrichr:
756 a comprehensive gene set enrichment analysis web server 2016 update. Nucleic Acids Res.
757 2016;44(W1):W90-7.
758 87. Gui B, Gui F, Takai T, Feng C, Bai X, Fazli L, et al. Selective targeting of PARP-2
759 inhibits androgen receptor signaling and prostate cancer growth through disruption of FOXA1
760 function. Proc Natl Acad Sci U S A. 2019;116(29):14573-82.
761 88. Jones D, Wade M, Nakjang S, Chaytor L, Grey J, Robson CN, et al. FOXA1 regulates
762 androgen receptor variant activity in models of castrate-resistant prostate cancer. Oncotarget.
763 2015;6(30):29782-94.
764 89. Andreu-Vieyra C, Lai J, Berman BP, Frenkel B, Jia L, Jones PA, et al. Dynamic
765 nucleosome-depleted regions at androgen receptor enhancers in the absence of ligand in prostate
766 cancer cells. Mol Cell Biol. 2011;31(23):4648-62.
767 90. Chen Z, Lan X, Thomas-Ahner JM, Wu D, Liu X, Ye Z, et al. Agonist and antagonist
768 switch DNA motifs recognized by human androgen receptor in prostate cancer. EMBO J.
769 2015;34(4):502-16.
770 91. Ye Z, Chen Z, Sunkel B, Frietze S, Huang TH, Wang Q, et al. Genome-wide analysis
771 reveals positional-nucleosome-oriented binding pattern of pioneer factor FOXA1. Nucleic Acids
772 Res. 2016;44(16):7540-54.

773 92. Strobeck MW, Knudsen KE, Fribourg AF, DeCristofaro MF, Weissman BE, Imbalzano
774 AN, et al. BRG-1 is required for RB-mediated cell cycle arrest. Proc Natl Acad Sci U S A.
775 2000;97(14):7748-53.
776 93. Zhang HS, Gavin M, Dahiya A, Postigo AA, Ma D, Luo RX, et al. Exit from G1 and S
777 phase of the cell cycle is regulated by repressor complexes containing HDAC-Rb-hSWI/SNF
778 and Rb-hSWI/SNF. Cell. 2000;101(1):79-89.
779 94. Naidu SR, Love IM, Imbalzano AN, Grossman SR, Androphy EJ. The SWI/SNF
780 chromatin remodeling subunit BRG1 is a critical regulator of p53 necessary for proliferation of
781 malignant cells. Oncogene. 2009;28(27):2492-501.
782 95. Stelloo S, Nevedomskaya E, Kim Y, Hoekman L, Bleijerveld OB, Mirza T, et al.
783 Endogenous androgen receptor proteomic profiling reveals genomic subcomplex involved in
784 prostate tumorigenesis. Oncogene. 2018;37(3):313-22.
785 96. Pomerantz MM, Li F, Takeda DY, Lenci R, Chonkar A, Chabot M, et al. The androgen
786 receptor cistrome is extensively reprogrammed in human prostate tumorigenesis. Nat Genet.
787 2015;47(11):1346-51.
788 97. Rueden CT, Schindelin J, Hiner MC, DeZonia BE, Walter AE, Arena ET, et al. ImageJ2:
789 ImageJ for the next generation of scientific image data. BMC Bioinformatics. 2017;18(1):529.
790 98. Schneider CA, Rasband WS, Eliceiri KW. NIH Image to ImageJ: 25 years of image
791 analysis. Nat Methods. 2012;9(7):671-5.
792 99. Liao Y, Smyth GK, Shi W. featureCounts: an efficient general purpose program for
793 assigning sequence reads to genomic features. Bioinformatics. 2014;30(7):923-30.
794 100. Bert SA, Robinson MD, Strbenac D, Statham AL, Song JZ, Hulf T, et al. Regional
795 activation of the cancer genome by long-range epigenetic remodeling. Cancer cell. 2013;23(1):9-
796 22.

797 101. Ramirez F, Ryan DP, Gruning B, Bhardwaj V, Kilpert F, Richter AS, et al. deepTools2: a
798 next generation web server for deep-sequencing data analysis. Nucleic Acids Res.
799 2016;44(W1):W160-5.

800

801 **FIGURE LEGENDS**

802

803 **Figure 1. *SMARCA4* (BRG1) is over expressed in prostate cancer**. A) *SMARCA4* gene
804 expression (logPRKM) in TCGA data (tumours n= 486, normal = 52) with tumour samples
805 separated by molecular subtype defined by the TCGA. *SMARCA4* expression is increased across
806 all groups, with subtypes ERG, ETV1, ETV4, IDH1, SPOP, and FOXA1 all significantly up
807 regulated, one-way ANOVA Dunnett's multiple comparison correction $**p<0.05$. B) *SMARCA4*
808 gene expression in prostate cell lines normalised to *18S* and relative to PrEC (n = 2). Significance
809 determined by one-way ANOVA with Tukey's multiple comparison correction $***p<0.001$. Bars
810 denote mean, and error bars are SD. C) Representative Western blot of BRG1 protein level in
811 prostate cell lines. Quantification above Western Blot by adjusted relative density normalized to
812 GAPDH and relative to PrEC. D) Expression of *SMARCA4* from RNA-seq in prostate cell lines
813 grouped as normal, cancer or transformed. The mean of each group was calculated, and a
814 significance was tested by one-way ANOVA Dunnett's multiple comparison correction,
815 $**p<0.05$.

816

817 **Figure 2. Loss of BRG1 results in a down regulation of gene expression.** A) Schematic of
818 temporal BRG1 knockdown model used for RNA-seq. Samples were collected at 72hrs (si-NT
819 control, si-*SMARCA4*-1 and si-*SMARCA4*-2) and 144hrs (si-NT, si-*SMARCA4*-1 and si-
820 *SMARCA4*-2) post siRNA transfection in duplicate for each condition at each time point (n=2).
821 Cells were transfected with either control siRNA (si-NT) or *SMARCA4* siRNA. B) *SMARCA4*
822 gene expression in control and post BRG1 depletion in the RNA-seq data, shown as transcripts

per million reads (TPM). Control siRNA for 72 and 144 hours are shown collectively as si-NT. *SMARCA4* expression is significantly down regulated at both time points, ****p<0.0001*. Bars denote mean, and error bars are SD. C) Representative Western blots of BRG1 and GAPDH protein levels at 72 and 144 hours post transfection. Adjusted relative density for BRG1 is calculated relative to GAPDH and normalized to the non-targeting control. Bars denote mean, and error bars are SD. D-E) Volcano plots of differentially expressed genes at 72 hours and 144 hours post knockdown. Significantly down regulated genes are blue and significantly up regulated genes for 72 and 144 hours post knockdown are shown in orange and red respectively. *SMARCA4* differential expression is highlighted in purple. Expression is shown as normalised log2 counts per million reads.

Figure 3. BRG1 regulates genes associated with prostate cancer. A) Heatmap illustrating RNA-seq differential gene expression data for up (n = 16) and down (n = 126) regulated genes common to both time points after BRG1 depletion. Expression is represented as the normalised row Z-score of TPM. B-D) *KLK2, VAV3 and PCAT-1* gene expression from the RNA-seq datasets shown as TPM. Bars denote mean, and error bars are SD. E) Gene set enrichment analysis using 'Enrichr' of differentially expressed genes that are common to both time points, showing the adjusted p-value (log 10, reversed x-axis) of significantly enriched transcription factor ChIP-seq from ChEA curated data *(p<0.05)*. F) Heatmap of BRG1, AR and FOXA1 ChIP-seq signal at BRG1 binding sites in LNCaP cells, +/- 2.5 kb from the centre of the binding site. Data is clustered into three groups by k-means. G) IGV images of the genes *KLK2*, *PCAT-1* and *VAV3*. Grey shaded regions contain ChIP-seq signal peaks for BRG1, AR and FOXA1.

Figure 4. BRG1 regulates genes involved the cell cycle. A) Gene set enrichment analysis using 'Enrichr' of down regulated genes at 144 hours post BRG1 knockdown. Enriched GO terms are classified as biological processes, cellular component or molecular function. Adjusted p-value (log

10, reversed x-axis) of the 10 most significant GO terms are shown. B) Heatmap of gene expression profiles from the top 40 differential cell cycle genes after BRG1 depletion. Expression is shown as the normalised row Z-score of transcripts per million reads (TPM), with blue indicating higher expression and red indicating lower expression. Genes involved in DNA replication initiation are indicated in blue. C-D) Gene expression from RNA-seq (TPM), of the MCM2-7 helicase components (top) and the Origin of Replication complex (ORC) subunits (bottom). Error bars denote mean and standard deviation. Bars denote mean, and error bars are SD. E) Representative Western blot showing protein levels of replication initiation genes MCM5, CDC6 and ORC6, along with CHK1, after 72 and 144 hours post BRG1 depletion. Error bars demonstrate SD. F) Quantification of Western blots demonstrating adjusted relative density to GAPDH (n = 2). G) Representative flow cytometry scatter of DAPI (x-axis) and EdU (y-axis) fluorescence intensity at 72 and 144 hours post BRG1 knockdown. G1 cells are shown by boxed gate. H) Percentage of cells in each phase of the cell cycle from flow cytometry data, error bars show standard deviation (n = 2). Error bars show SD.

Supplementary Figure 1. A) SWI/SNF subunit gene expression (TPM) from RNA-seq data. All subunits, except *SMARCA4* (shown in Figure 2A), are not significantly altered. Bars denote mean, and error bars are SD. B) PCA plot characterising the trend in expression profiles between the non-targeting control and after BRG1 knockdown. Each point on the plot represents an RNA-seq sample. Samples are separated by principal components 1 and 2, which together explain 58.37 % of the variance between the samples. C) Number of skipped exons at 72 hours and 144 hours after BRG1 knockdown with si-*SMARCA4*-1 (black) and si-*SMARCA4*-2 (grey). D) Number of retained introns at 72 hours and 144 hours post BRG1 depletion with si-*SMARCA4*-1 (black) and si-*SMARCA4*-2 (grey). E) Sashimi plot of exons one and two of the *KLK3* gene in the non-targeting and 144 hour knockdown RNA-seq data. Arcs represent the number of split reads across the exons. Lower numbers represent increased retention of the first intron after BRG1 knockdown.

875

876 **Supplementary Figure 2.** A) Expression of *KLK2, PCAT-1 and VAV3* in prostate cell lines
877 grouped as normal, cancer or transformed. B) *AR* and *FOXA1* gene expression from the RNA-seq
878 datasets shown as TPM. Bars denote mean, and error bars are SD.

879

880 **Supplementary Figure 3.** A) Heatmap of replication gene promoters, +/- 5kb from the
881 transcription start site. B) IGV images of the genes *CDC45*, *ORC6* and *MCM2*. Grey shaded
882 regions contain ChIP-seq signal peaks for BRG1 and active histone modifications.

FIGURE 1

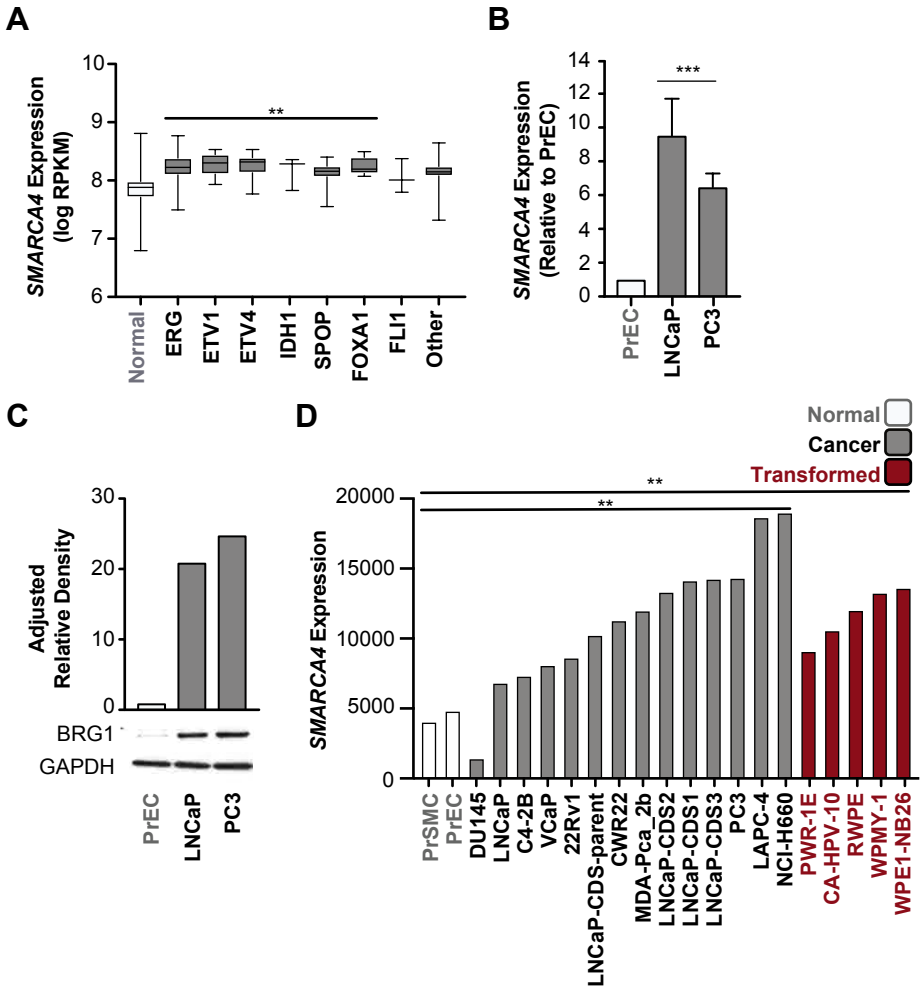
A
SMARCA4 Expression (log RPKM)
10
9
8
7
6
**
Normal
ERG
ETV1
ETV4
IDH1
SPOP
FOXA1
FLI1
Other
B
SMARCA4 Expression (Relative to PrEC)
14
12
10
8
6
4
2
0
***
PrEC
LNCaP
PC3
C
Adjusted Relative Density
30
20
10
0
BRG1
GAPDH
PrEC
LNCaP
PC3
D
Normal
Cancer
Transformed
SMARCA4 Expression
20000
15000
10000
5000
0
**
**
PrSMC
PrEC
DU145
LNCaP
C4-2B
VCaP
22Rv1
LNCaP-CDS-parent
CWR22
MDA-Pca_2b
LNCaP-CDS2
LNCaP-CDS1
LNCaP-CDS3
PC3
LAPC-4
NCI-H660
PWR-1E
CA-HPV-10
RWPE
WPMY-1
WPE1-NB26

FIGURE 2

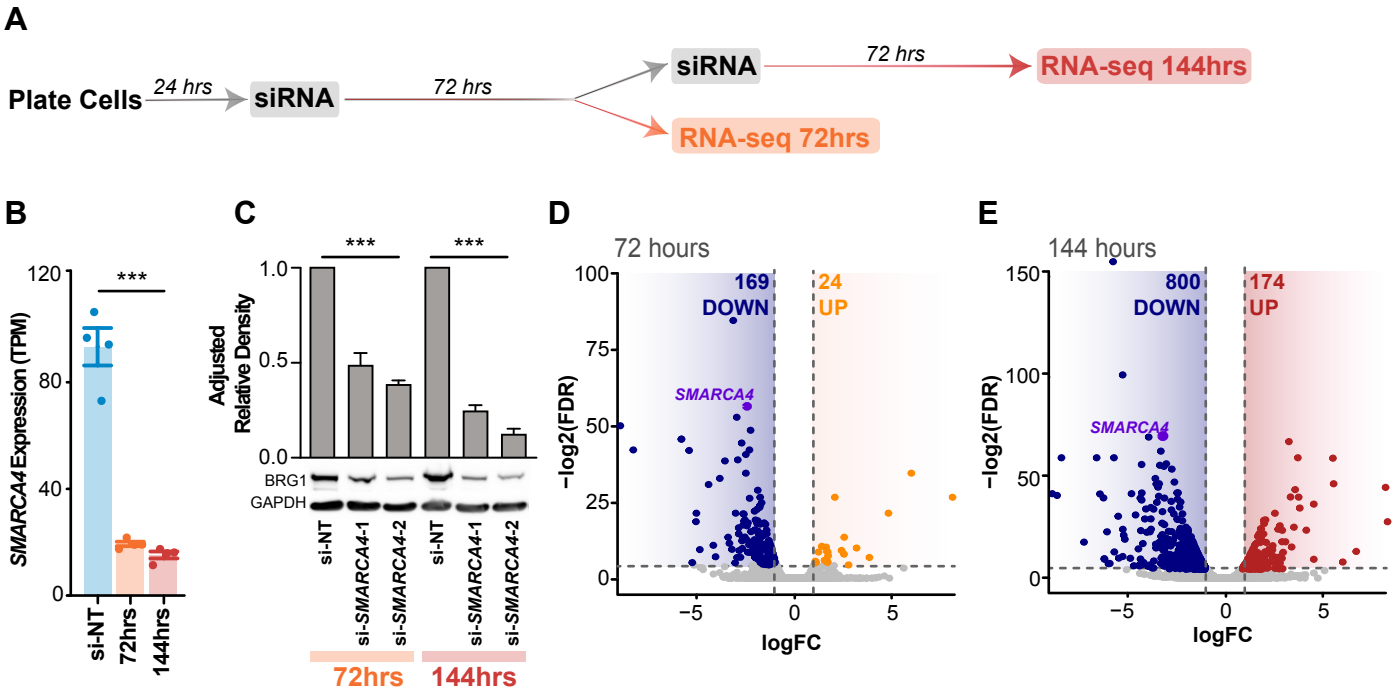
A
Plate Cells
24 hrs
siRNA
72 hrs
siRNA
72 hrs
RNA-seq 144hrs
RNA-seq 72hrs
B
SMARCA4 Expression (TPM)
120
80
40
0
***
si-NT
72hrs
144hrs
C
Adjusted Relative Density
1.0
0.5
0.0
***
***
BRG1
GAPDH
si-NT
si-SMARCA4-1
si-SMARCA4-2
si-NT
si-SMARCA4-1
si-SMARCA4-2
72hrs
144hrs
D
72 hours
169
DOWN
24
UP
SMARCA4
−log2(FDR)
100
75
50
25
0
−5
0
5
logFC
E
144 hours
800
DOWN
174
UP
SMARCA4
−log2(FDR)
150
100
50
0
−5
0
5
logFC

FIGURE 3

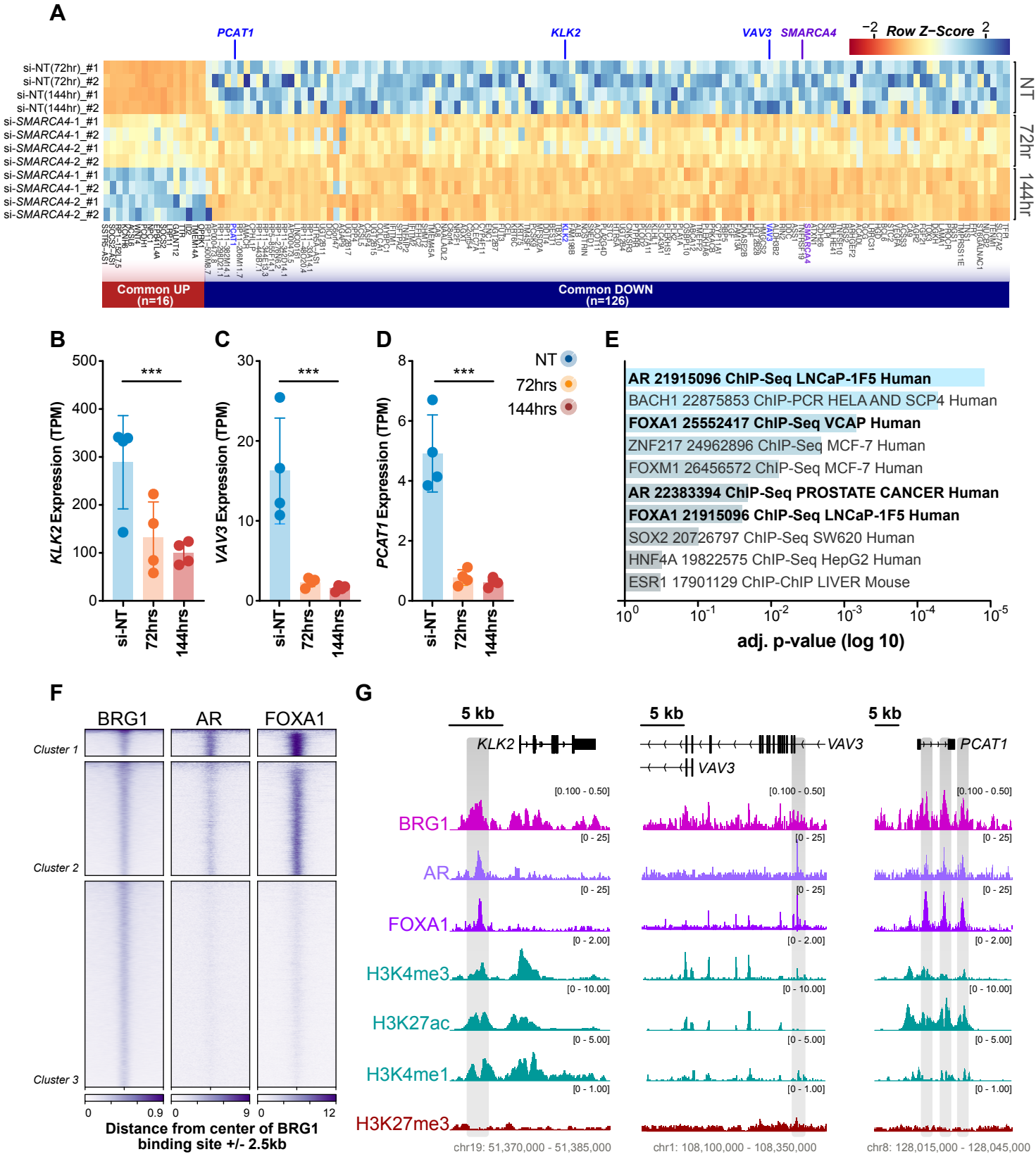
A
PCAT1
KLK2
VAV3
SMARCA4
Row Z-Score
si-NT(72hr)_#1
si-NT(72hr)_#2
si-NT(144hr)_#1
si-NT(144hr)_#2
si-SMARCA4-1_#1
si-SMARCA4-1_#2
si-SMARCA4-2_#1
si-SMARCA4-2_#2
si-SMARCA4-1_#1
si-SMARCA4-1_#2
si-SMARCA4-2_#1
si-SMARCA4-2_#2
NT
72hr
144hr
Common UP (n=16)
Common DOWN (n=126)
B
KLK2 Expression (TPM)
***
si-NT
72hrs
144hrs
C
VAV3 Expression (TPM)
***
D
PCAT1 Expression (TPM)
***
NT
72hrs
144hrs
E
AR 21915096 ChIP-Seq LNCaP-1F5 Human
BACH1 22875853 ChIP-PCR HELA AND SCP4 Human
FOXA1 25552417 ChIP-Seq VCAP Human
ZNF217 24962896 ChIP-Seq MCF-7 Human
FOXM1 26456572 ChIP-Seq MCF-7 Human
AR 22383394 ChIP-Seq PROSTATE CANCER Human
FOXA1 21915096 ChIP-Seq LNCaP-1F5 Human
SOX2 20726797 ChIP-Seq SW620 Human
HNF4A 19822575 ChIP-Seq HepG2 Human
ESR1 17901129 ChIP-ChIP LIVER Mouse
adj. p-value (log 10)
F
BRG1
AR
FOXA1
Cluster 1
Cluster 2
Cluster 3
Distance from center of BRG1 binding site +/- 2.5kb
G
5 kb
KLK2
VAV3
PCAT1
BRG1
AR
FOXA1
H3K4me3
H3K27ac
H3K4me1
H3K27me3
chr19: 51,370,000 - 51,385,000
chr1: 108,100,000 - 108,350,000
chr8: 128,015,000 - 128,045,000

FIGURE 4

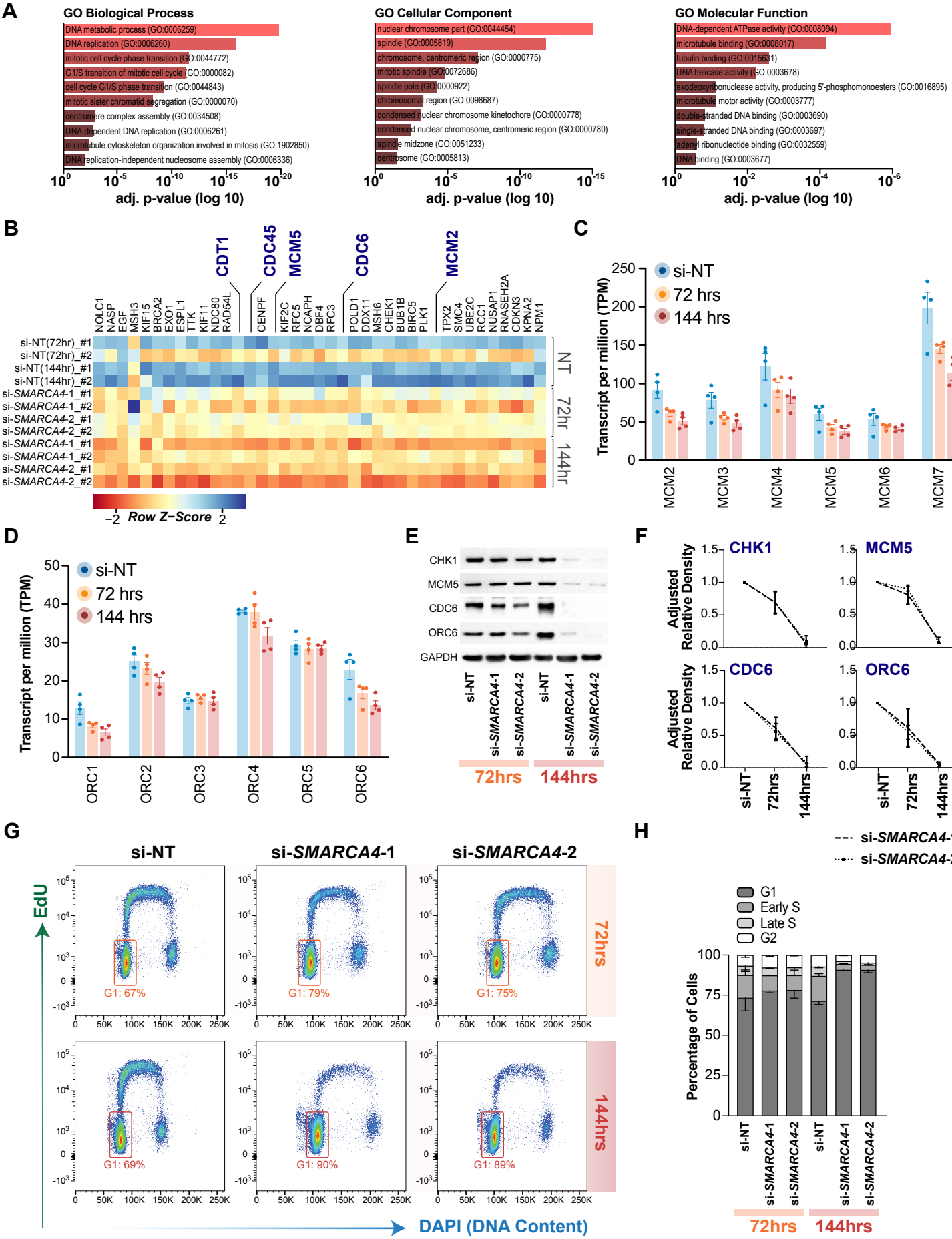
A
GO Biological Process
DNA metabolic process (GO:0006259)
DNA replication (GO:0006260)
mitotic cell cycle phase transition (GO:0044772)
G1/S transition of mitotic cell cycle (GO:0000082)
cell cycle G1/S phase transition (GO:0044843)
mitotic sister chromatid segregation (GO:0000070)
centromere complex assembly (GO:0034508)
DNA-dependent DNA replication (GO:0006261)
microtubule cytoskeleton organization involved in mitosis (GO:1902850)
DNA replication-independent nucleosome assembly (GO:0006336)
adj. p-value (log 10)
GO Cellular Component
nuclear chromosome part (GO:0044454)
spindle (GO:0005819)
chromosome, centromeric region (GO:0000775)
mitotic spindle (GO:0072686)
spindle pole (GO:0000922)
chromosomal region (GO:0098687)
condensed nuclear chromosome kinetochore (GO:0000778)
condensed nuclear chromosome, centromeric region (GO:0000780)
spindle midzone (GO:0051233)
centrosome (GO:0005813)
adj. p-value (log 10)
GO Molecular Function
DNA-dependent ATPase activity (GO:0008094)
microtubule binding (GO:0008017)
tubulin binding (GO:0015631)
DNA helicase activity (GO:0003678)
exodeoxyribonuclease activity, producing 5'-phosphomonoesters (GO:0016895)
microtubule motor activity (GO:0003777)
double-stranded DNA binding (GO:0003690)
single-stranded DNA binding (GO:0003697)
adenyl ribonucleotide binding (GO:0032559)
DNA binding (GO:0003677)
adj. p-value (log 10)
B
CDT1
CDC45
MCM5
CDC6
MCM2
NOLC1 NASP EGF MSH3 KIF15 BRCA2 EXO1 ESPL1 TTK KIF11 NDC80 RAD54L CENPF KIF2C RFC5 NCAPH DBF4 RFC3 POLD1 DDX11 MSH6 CHEK1 BUB1B BIRC5 PLK1 TPX2 SMC4 UBE2C RCC1 NUSAP1 RNASEH2A CDKN3 KPNA2 NPM1
si-NT(72hr)_#1
si-NT(72hr)_#2
si-NT(144hr)_#1
si-NT(144hr)_#2
si-SMARCA4-1_#1
si-SMARCA4-1_#2
si-SMARCA4-2_#1
si-SMARCA4-2_#2
NT
72hr
144hr
−2 Row Z−Score 2
C
si-NT
72 hrs
144 hrs
Transcript per million (TPM)
MCM2 MCM3 MCM4 MCM5 MCM6 MCM7
D
si-NT
72 hrs
144 hrs
Transcript per million (TPM)
ORC1 ORC2 ORC3 ORC4 ORC5 ORC6
E
CHK1
MCM5
CDC6
ORC6
GAPDH
si-NT si-SMARCA4-1 si-SMARCA4-2 si-NT si-SMARCA4-1 si-SMARCA4-2
72hrs 144hrs
F
CHK1
MCM5
CDC6
ORC6
Adjusted Relative Density
si-NT 72hrs 144hrs
G
si-NT
si-SMARCA4-1
si-SMARCA4-2
EdU
DAPI (DNA Content)
G1: 67%
G1: 79%
G1: 75%
G1: 69%
G1: 90%
G1: 89%
72hrs
144hrs
H
si-SMARCA4-1
si-SMARCA4-2
G1
Early S
Late S
G2
Percentage of Cells
si-NT si-SMARCA4-1 si-SMARCA4-2 si-NT si-SMARCA4-1 si-SMARCA4-2
72hrs 144hrs